# LIGHTING UP THE REGOLITH WITH ELECTRICAL GEOPHYSICS

**Dr Graham Heinson[1], Mr Hashim Carey[1] and Mr Mike Sexton[2]**

*[1]CRC LEME, School of Earth and Environmental Sciences, University of Adelaide, Adelaide SA 5005*
*[2]Newmont Australia Ltd., Adelaide SA 5001*
graham.heinson@adelaide.edu.au

## ABSTRACT

Downhole-to-surface electrical geophysics provides a rapid and cheap approach to determine the spatial extent of mineralisation beneath cover. In this method, sometimes known as mise-à-la-masse, a downhole current electrode provides a source, and a roving surface electrode measures the resulting electrical potential. The method is particularly applicable at brown-fields exploration sites where mineralisation or alteration has been intersected by one or more drill holes, as it indicates continuity of electrical interconnection of mineralised regions, extending exploration targets away from drill holes.

To date, interpretation methods have been mostly qualitative, involving plots of gridded surface electrical potential data, with little or no processing. This CRC LEME funded study provides a quantitative means of interpreting data, through (a) a numerical approach to separate the surface potential into contributions from the source current electrode and sub-surfaces charges at resistivity boundaries in the Earth, and (b) a simple three-dimensional (3D) imaging method to determine the lateral and vertical extent of the conductive mineralisation. The methods described work in both the case where a drill hole intersects mineralisation and the source current electrode is directly connected to the conductive ore, and in the "near-miss" scenario in which the drill hole does not intersect mineralisation. Data from the Golden Grove VMS deposit in Western Australia are shown for example.

## INTRODUCTION

The downhole-to-surface electrical technique is under utilised given the simplicity of the method, and the possible information that can be extracted from resulting data (Ketola 1972). Data are generally collected in a pole-pole configuration (Eloranta 1985) by placing a current electrode in contact with, or close by, a conductive target, either downhole or at an outcrop. A return current electrode is located as far as possible to simulate a point current source (Figure 1). Surface potentials are mapped using a roving electrode relative to a reference potential electrode placed some distance away.

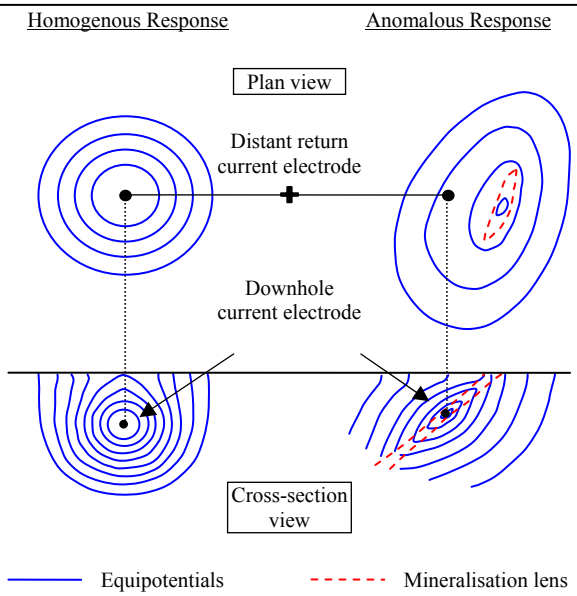


**Figure 1**: Surface and sub-surface equipotential contours for (left figure) homogenous media, and (right figure) anomalous structure, such as a mineralised lens.

Equipotentials about an energised current electrode are approximately spherical in a homogenous and isotropic half-space. Surface potential responses are symmetrical, centred above the current electrode (Figure 1). Any resistivity changes within the Earth distort the potentials, and on the surface the maximum potentials are centred over the top of the conductive body. Surface potentials may therefore indicate the lateral and depth extent of a conductive structure and can provide information on the continuity of ore between borehole intersections or outcrops. However, data do not

readily provide unique depth constraints to the target, as is the case with all surface potential field measurements.

## LOCALE AND GEOLOGICAL DESCRIPTION

Field data were obtained by Newmont Australia at the Scuddles Mine, Golden Grove tenement, Western Australia (approximately 225 km inland from Geraldton) (Boyd and Frankcombe 1994). The location hosts a base metals operation involving a volcanogenic massive sulphide (VMS), with the primary target being a massive pyrite. Covering the region is a conductive weathered overburden of thickness 80-100 m. The target is a conductive band 80 m wide, steeply dipping 80° to the west, striking north-south, with a plunge of 5° to the north (Boyd and Frankcombe 1994). The conductive body has been extensively drilled, and downhole electrical surveys conducted at numerous drill holes. The region has low topographical relief with the only prominent feature being a low-lying hill situated over the ore body, aptly named Gossan Hill. More details of the field area are given by Carey (2003).

## METHODS

The area surveyed measured 750 by 1000 m. The transmitter used was an Iris VIP-4000 that supplied between 2-5 A on a two second cycle at 200 volts. The receiver used was an Elrec 6 IP. The distant return electrodes were placed more than 2 km from the survey area. Most surveys were conducted in a pole-pole configuration with the current electrode placed at the depth of lowest resistivity of the target formation to ensure a good coupling to the conductive body. However, several surveys were also conducted in a near-miss configuration, where the current electrode was outside the target formation's known depth, as identified from drill logs.

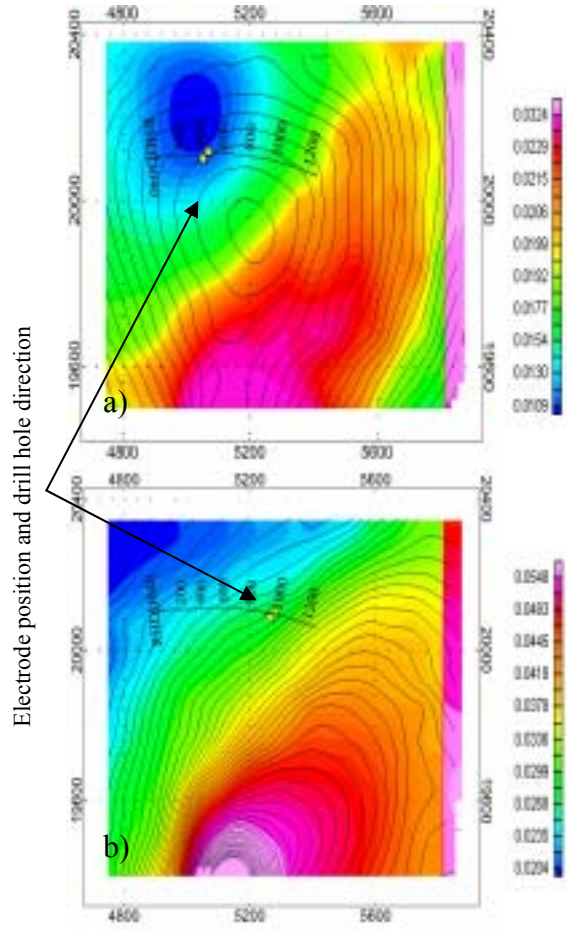


**Figure 2** (a) Line contours of observed surface potentials (current electrode at 450 m), superimposed on a colour map of residual potentials after the removal of the electrode effect. (b) As for (a) but for the current electrode at 850 m.

Electrode Effect Removal

Electric potential fields produced by a buried current electrode inside any complex geologic resistivity structure can be described as part of a geoelectric construct, where the potential U at point P is due to integral sum of all point current sources and or sinks (Keller and Frischknecht 1966).

$$U(P) = \frac{1}{2\pi}\left[\int_v \frac{\rho \,\mathrm{div}\,\mathbf{J}}{r}\,dV + \int_v \frac{\mathbf{E}\cdot \mathrm{grad}\,\rho}{\rho r}\,dV\right] \quad (1)$$

In equation (1) **J** and **E** are the electric current density and electric field vectors, r is the distance from point P to the volume element dV, and ρ is the resistivity. The **first integral** is the primary input to U(P) from a divergence of electric current density (div **J**) from the downhole current electrode; the **second integral** is due to the electric charges accumulating at any gradient in electrical resistivity (grad ρ) within the sub-surface.

From equation (1) we can calculate the first integral simply using the image-current technique (Telford et al. 1990) from a buried electrode in a homogenous half-space. Assuming we can measure U(P) on the surface of the Earth, we can re-arrange equation (1) to yield just the contribution due to subsurface resistivity changes $U^r(P)$:

$$U^r(P) = \int_V \frac{\mathbf{E} \cdot \operatorname{grad} \rho}{\rho r} dV = \left[ \int_V \frac{\rho \operatorname{div} \mathbf{J}}{r} dV - 2\pi U(P) \right] \quad (2)$$

This technique was applied to sets of data from the same drill hole but at different depths of 450 m and 850 m. The gridded surface potentials from the shallow survey are shown as solid contour lines (Figure 2a), and are significantly different to the contours from the deep survey (Figure 2b). The shallower potential response is a broad anomaly, with highest values to the southeast of the current electrode location, while the deeper response yields the highest values far to the south of the current electrode. The shape of the surface potential contours is also different.

The current electrode effect was modelled using the image-current technique (Telford et al. 1990) with a half-space of 1000 Ω.m. Modelled surface potentials were subtracted from observations, and residual potentials are shown in Figures 2a,b as colour maps. In Figure 2a, residual potentials from the 450 m current electrode case no longer have a peak anomaly centred in the survey area; the maximum potentials now occurs on the southern margin of the survey, similar to field data collected with the deeper current electrode. Applying the same technique for the case with the current electrode at 850 m in Figure 2b shows minimal change to the surface potentials. We note now that the residual potential maps in Figures 2a and 2b are quite similar, indicating that the sources of the residual potentials are due to subsurface resistivity variations and not the location of the source current electrode.

Image Reconstruction Method

A strategy to determine quantitative information from the residual surface potentials has been developed by Patella (1997) and Hämmann et al. (1997). Surface potentials can be represented by the integral sum of potentials from all sub-surface charges that occur at locations where there is a resistivity gradient (ie. grad $\rho \neq 0$). An electric charge at a point in the sub-surface (x,y,z) generates a modelled potential $V^m$ at a surface location (a,b,0) that has the form

$$V^m(a,b,0) = \frac{2\rho I}{4\pi\sqrt{(x-a)^2 + (y-b)^2 + z^2}} \quad (3)$$

where I is the current at the charge location, and ρ is the average resistivity of the sub-surface. We can define a cross-correlation coefficient $\hat{C}(x,y,z)$ between the modelled potentials $V^m$ and residual potentials $U^r$ after electrode effects have been removed, for all measurement positions (a,b,0) as

$$\hat{C}(x,y,z) = \sum_a \sum_b V^m U^r \quad (4)$$

Equation (4) can be normalised by the square-root of the sum-squared components of observed and modelled potentials as

$$C_{norm}(x,y,z) = \frac{\hat{C}(x,y,z)}{\sqrt{\sum_a \sum_b V^2 \sum_a \sum_b U^2}} \quad (5)$$

We note that the normalised function $C_{norm}$ has no dependence on I or ρ, only on the distances between the point source and the surface locations. The function $C_{norm}$ is defined to range between –1 and 1; strong positive correlations (0.8 to 1) indicate the probable location of positive point-charges, while negative correlations (-0.8 to -1) show probable negative point-charged sources. Numerical scanning through a range of source locations (x,y,z) in equation (5) produce a matrix that can be contoured as a 'map' of sources correlations.

Figure 3 shows two iso-surfaces of the normalised correlation function $C_{norm}$ for the residual potentials in Figure 2a. The upper iso-surface is for $C_{norm} = 0.9$; while the more spherical surface is for $C_{norm} =$

0.95 (implying a 95% correlation with the observed residual potentials). The figure is orientated with the southern margin on the right side, suggesting that the ore body is at a depth of about 500 m, and is not continuous from south to north, possibly terminated by east-west striking faults. The choice of a suitable cut-off value of $C_{norm}$ is somewhat arbitrary. However, we find experimentally that 0.95 is often appropriate.

## CONCLUSION

We conclude that the use of gridded maps of surface potential is outmoded and insufficient, as the potential field due to the electrode can significantly distort and dominate the surface response. With an image current approach, it is very easy to remove the electrode potential, and the residual potential map is a better representation of the subsurface charge distribution that occurs at resistivity boundaries. Rather than 3D forward and inverse modelling, we recommend an alternative approach of defining a 3D scanning function and determining a spatial correlation with the measured fields. As targets are bounded by changes in resistivity, it is of interest to know where charges are located spatially rather than in terms of their electrical potential response.

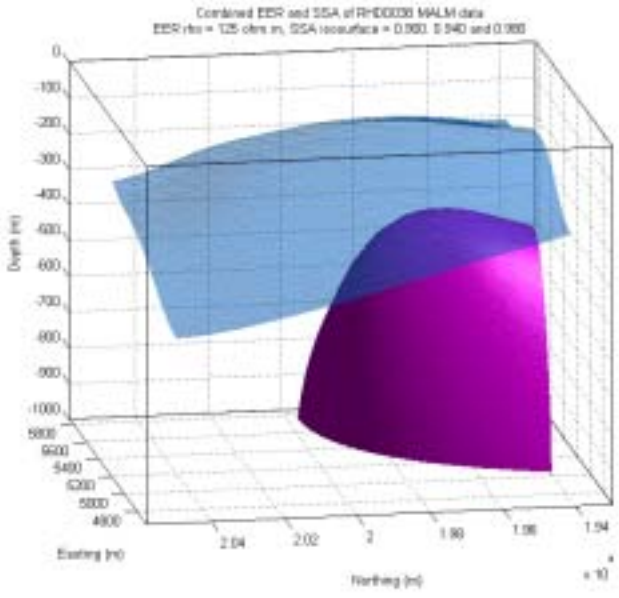

**Figure 3**: Iso-surfaces of the correlation function $C_{norm}$ for the area of survey shown in Figure 2. The figure is orientated such that the north-direction is from right to left. The two surfaces are for $C_{norm}$ = 0.9 (upper), and $C_{norm}$ = 0.95 (lower).


## ACKNOWLEDGMENTS

We thank Newmont Australia Ltd for financial and in-kind support during this project. Additional funding was supplied from the CRC LEME. The work in this abstract formed part of an M.Sc. thesis undertaken at the University of Adelaide (Carey, 2003).


## REFERENCES


BOYD G. & FRANKCOMBE K.F. 1994. Geophysical Responses over the Scuddles VMS deposit. *Geophysical Signatures of Western Australian Mineral Deposits*, Ed. Dentith, M., pp 133 – 144.

CAREY H. 2003. *Augmented Mise-a-la_Masse Interpretation Using Rapid Numerical Methods*, MSc. Thesis, University of Adelaide, pp 147.

ELORANTA E.H. 1985. A Comparison between Mise-à-la-Masse anomalies obtained by pole-pole and pole-dipole electrode configurations. *Geoexploration* **23** 471-481.

HÄMMANN M., MAURER H.R., GREEN A.G., & HORSTMEYER H. 1997, Self potential image reconstruction: Capabilities and limitations. *Journal of Environmental and Engineering Geophysics* **2** 21-36.

KELLER G.V. & FRISCHKNECHT F.C. 1966. *Electrical Methods in Geophysical Prospecting*. Pergamon Press, Inc.

KETOLA M. 1972. Some points of view concerning Mise-à-la-Masse measurements. *Geoexploration* **10** 1 – 21.

PATELLA D. 1997. Introduction to ground surface self-potential tomography. *Geophysical Prospecting* **45** 653-681.

TELFORD W.M., GELDART L.P. & SHERIFF R.E. 1990. *Applied Geophysics 2nd Edition*. Cambridge University Press.